Numerical Forecast of Fog – Central Solutions

Binbin Zhou[1,2] , Jun Du[1,2] , Brad Ferrier[1,2], Jeff McQueen[2] and Geoff Dimego[2]

[1] Science Application International Corporation
[2] Environmental Modeling Center, NCEP, NWS, NOAA

Abstract

Progress in the operational forecast of fog has been slow, although numerical weather prediction (NWP) models have been upgraded for several generations at NCEP and other weather forecast centers (WFCs). Conventional NWP models are not reliable in predicting local-scale fogs near the surface. Sophisticated fog models are usually applied to limited locations. For an operational forecast over large domains, sophisticated fog models require significant computing resources beyond the capacity of most WFCs. Under current WFC computing conditions, a realistic approach is to diagnose fog from NWP models without significantly increasing the computational burden. In this paper, two diagnostic solutions are presented. The first solution is based on the diagnosis of surface clouds and *RH* from the model's post processor. This method has been implemented in NCEP's Short Range Forecast Ensemble System (SREF). The uncertainties involved in this solution can be addressed by predicting the probability of fog occurrence. The drawback of this approach is that it only predicts fog occurrence but not fog intensity or liquid water content (LWC), which is required for the computation of visibility. The second solution not only diagnoses the fog conditions but also resolves the fog LWC using an asymptotic LWC formulation obtained from singular perturbation methodology. This solution could also be potentially applied in NWP models. In this paper, the SREF ensemble fog forecast is introduced and subjectively verified with NOAA NESDIS fog/low-cloud detections. The second solution is briefly presented and its applications are only tentatively discussed since it needs more experimentation before possible implementation.

1. Introduction

Operational fog forecasting over large domains is notoriously difficult. The reasons are: (1) Conventional coarse grid NWP models are not adequate for local scale fog prediction; (2) Conventional NWP models are not specifically designed for fog prediction and the cloud parameterization schemes in the models function well only for clouds at high levels and not for fog near the surface. (Stoelinga and Warner 1999, Müller 2005); and (3) the computing resources at most weather forecast centers are limited.

Corresponding author address: Binbin Zhou, NCEP/EMC, 5200 Auth Rd. Camp Springs MD 20746, Email: Binbin.Zhou@noaa.gov

Most fog predictions now are local solutions, in which a very complicated 1D or 2D fog model is run locally at a selected point (such as an airport) and forced by a background mesoscale model. For operational forecasts over large domains like the Continental U.S. (CONUS), this approach is time-consuming and not applicable with currently available computing resources. Under current computing conditions, a realistic approach would be to find a way to diagnose fog without significantly increasing the operational forecast time. Recently, we have developed a fog ensemble prediction product based on the post processor of NCEP SREF. This system predicts the fog occurrence probability by diagnosing

the fog conditions from the SREF ensemble members. However, there is no fog intensity forecast from this product. The reason for that is that the operational models were not specifically designed for fog and there is no fog physics involved in the LWC computation. To improve this product, we suggested a new method to resolve the fog LWC from the post processor. This method is based on an asymptotic analysis of steady fog by Zhou (2006). The asymptotic solution is one-dimensional and does not consider horizontal advection. To apply this work to large domains, it has to be extended to two dimensions to include the advection. With such an extension, fog conditions and the LWC at each saturated grid point can be diagnosed or resolved based on the outputs from the operational models.

In this paper, we first present the SREF ensemble fog forecast and then discuss the asymptotic method. Verification of the fog forecast is extremely difficult due to a lack of routinely observed fog data for large domains. One solution is verification using satellite data. Recently NOAA NESDIS developed fog/low-cloud detection techniques and now routinely produces fog detection images. See http://www.orbit.nesdis.noaa.gov/smcd/opdb/aviation/fog.html for details. We will present a subjective verification of the SREF ensemble fog forecasts using the NESDIS fog detections. The asymptotic method has not yet been implemented at NCEP, but how to apply it in operational models is tentatively discussed in this paper.

2. Ensemble forecast solution

2.1. SREF ensemble fog forecast

The SREF fog forecast is generated from SREF system, which has been operational since 2001 (Du and Tracton, 2001). The current SREF system was built with four base models including the Eta, WRF-ARW, WRF-NMM and RSM, running twice a day (09Z and 21Z) over CONUS, Alaska and Hawaii out to 87 forecast hours with output every 3 hours. Perturbed initial conditions (IC, breeding method) as well as multiple convection schemes with the same lateral boundary conditions (LBC) and land surface model (LSM), are used to generate a total of 21 ensemble members, including 10 Eta members, 3 WRF-ARW members, 3 WRF-NMM members and 5 RSM members. In 2004, the SREF system was extended to include aviation weather forecasts (Zhou et al. 2004). Recently, a fog occurrence probability forecast was developed from this system. The daily fog forecast is displayed at http://wwwt.emc.ncep.noaa.gov/mmb/SREF_avia/FCST/AVN/web_site/fog/fog_com_09z_prb.htm. The web graphic interface is shown in Figure 1. The configurations of the 21 members in the SREF system are listed in Table 1 (Du et al. 2006).

Table 1. SREF ETA member's configurations

Models/Dyn Core	Physics	Res	Configuration	Membership	Base IC	LBC	LSM
Eta	BMJ	32km/60	N America/hydro	3 (1 ctl, 2 bred)	NDAS	GENS	NOAH
Eta	BMJ-SAT	32km/60	N America/hydro	2 (2 bred)	NDAS	GENS	NOAH
Eta	KF	32km/60	N America/hydro	3 (1 ctl, 2 bred)	NDAS	GENS	NOAH
Eta	KF-DET	32km/60	N America/hydro	2 (2 bred)	NDAS	GENS	NOAH
WRF NMM	NCEP/BMJ	40km/52	N Am/non-hydro	3 (1 ctl, 2 bred)	GDAS	GENS	NOAH
WRF ARW	NCAR/KF	45km/36	N Am/non-hydro	3 (1 ctl, 2 bred)	GDAS	GENS	NOAH
RSM	SAS	45km/28	N America/hydro	3 (1 ctl, 2 bred)	GDAS	GENS	NOAH
RSM	RAS	45km/28	N America/hydro	2 (1 ctl, 2 bred)	GDAS	GENS	NOAH

The symbols in Table 1 are as follows: BMJ for Bette-Miller-Janjic scheme, BMJ-SAT for BMJ with saturated profiles, KF for Kain-Fritsch, KF-DET for KF with detrainment, 32km/60 for 32km horizontal resolution with 60 vertical levels, ctl for the control member, '2 bred' for one pair of perturbations (positive/negative pair), RSM for Regional Spectral Model, RAS for Relaxed Arakawa-Schubert scheme, SAS for Simplified Arakawa-Schubert scheme, NDAS for NAM (North American Mesoscale) Data Assimilation System, GDAS for GFS (Global Forecast System) Data Assimilation System, and GENS for Global ENsemble System. The fog occurrence probability at each grid point is computed from the "yes/no" diagnosis from each ensemble member using the following cloud and *RH* thresholds:

(1) *RH* at 2m = 100%, and
(2) cloud base < 10 m and cloud top < 300 m

Then the ensemble fog occurrence probability distributions over CONUS are computed based on the occurrence counts out of the 21 members.
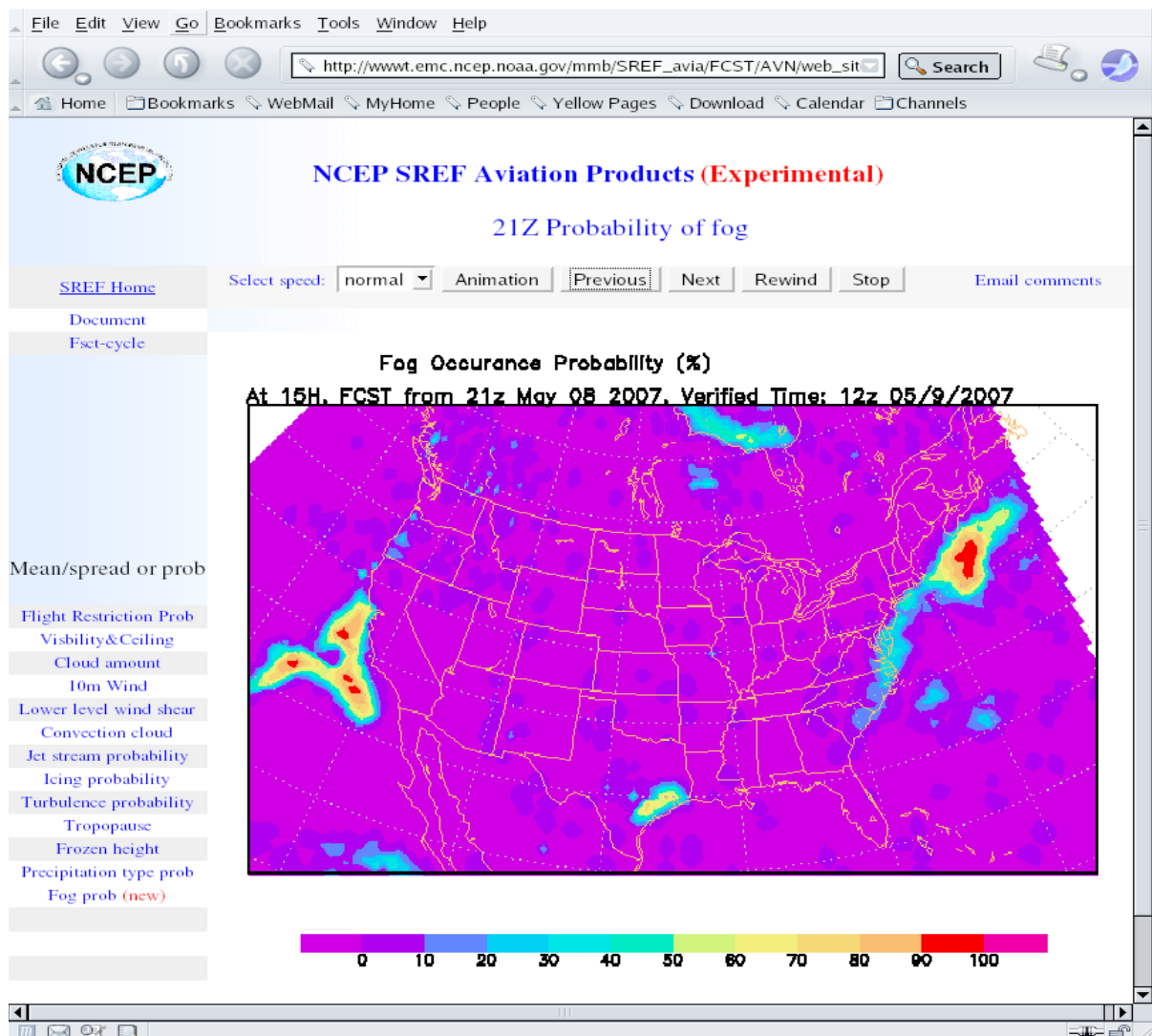
Figure 1. NCEP SREF fog ensemble forecast web interface.

2.2. Examples of SREF fog forecast

The SREF fog ensemble forecast was conducted experimentally for more than one year. Figure 2 is an example of fog probability distributions at different forecast times over CONUS on May 4th and 5th, 2007. This example illustrates several fog episodes in eastern Canada, in the region between Texas and Oklahoma, along the southern Texas coast, along the East Coast between Florida and Georgia, and in the area of northern Missouri-southern Illinois. The ocean and coastal fogs are marine fogs, while the types of the land fogs are not exactly known. The temporal evolutions of the fogs indicated that the marine fogs could linger several days without being completely dispersed, even during daytime, while the persistence of the land fogs strongly relied on the diurnal cycles of forecast time. The land fogs formed at night and dissipated soon after daybreak. This implies that the land fogs could be radiation fog, or an advection-radiation hybrid fog where both advection and radiation played a role. For example, the land fog episodes over inland Texas and Oklahoma only emerged around 12Z (05:00 Central Time) on May 4th and then dispersed after sunrise. But the marine fog over the Texas coast maintained itself both day and night for more than two days, although its intensity reduced a little during the daytime. Comparing the areas covered by marine fogs and land fogs, one can observe that the marine fogs covered much larger areas than the land fogs did. Such a difference in coverage between marine fog and land fog is due to their different formation mechanisms. For a marine fog, its formation depends on wind direction controlled by a synoptic weather system over a significantly colder or warmer ocean (Lewis et al. 2004), while land fog formation is strongly controlled by local factors such as humidity, local winds, radiation, surface properties and topography.

The SREF ensemble forecast mean of sea level pressure, 2m temperature and 10m wind speeds over COUNUS on May 4th and 5th are illustrated in Figure 3, which shows a strong high pressure system centered over eastern Canada followed by a weak low pressure system in the west over Colorado and Utah. In such a synoptic weather pattern, the moist air from the south was consistently transported by the southerly flow from the Gulf Mexico to south Texas, where the warm moist air met the cold coast. This is the reason for the formation of marine fog over Texas coast. The moist air continuously moved northward and inland with southerly winds and was further cooled by the gradually cooler land from south to north, as was indicated by a strong temperature gradient over the Texas-Oklahoma regions. Because the low pressure system over Colorado-Utah was still very weak on 4th, the winds over Oklahoma were very light. As a result, the moisture from the south stagnated there. The accumulated moisture over inland Texas and Oklahoma was further cooled by longwave radiation on the night of May 3rd, leading to the formation of an advection-radiation hybrid fog on the morning of May 4th.

The synoptic weather pattern on the second day (May 5th) changed due to the strengthening of the low pressure system to the west of Oklahoma. The weakening of the temperature gradient and increase in the surface temperature over Oklahoma-Texas meant the inland surface air layer had warmed. As a result, there was no land fog over Texas-Oklahoma on the second day, but the marine fog still lingered along the Texas coast. Since the eastern CONUS was still strongly controlled by the high pressure system and wind speeds were still weak over northern Missouri-southern Illinois, radiation fog formed on the morning of May 5th. It dissipated soon after sunrise.
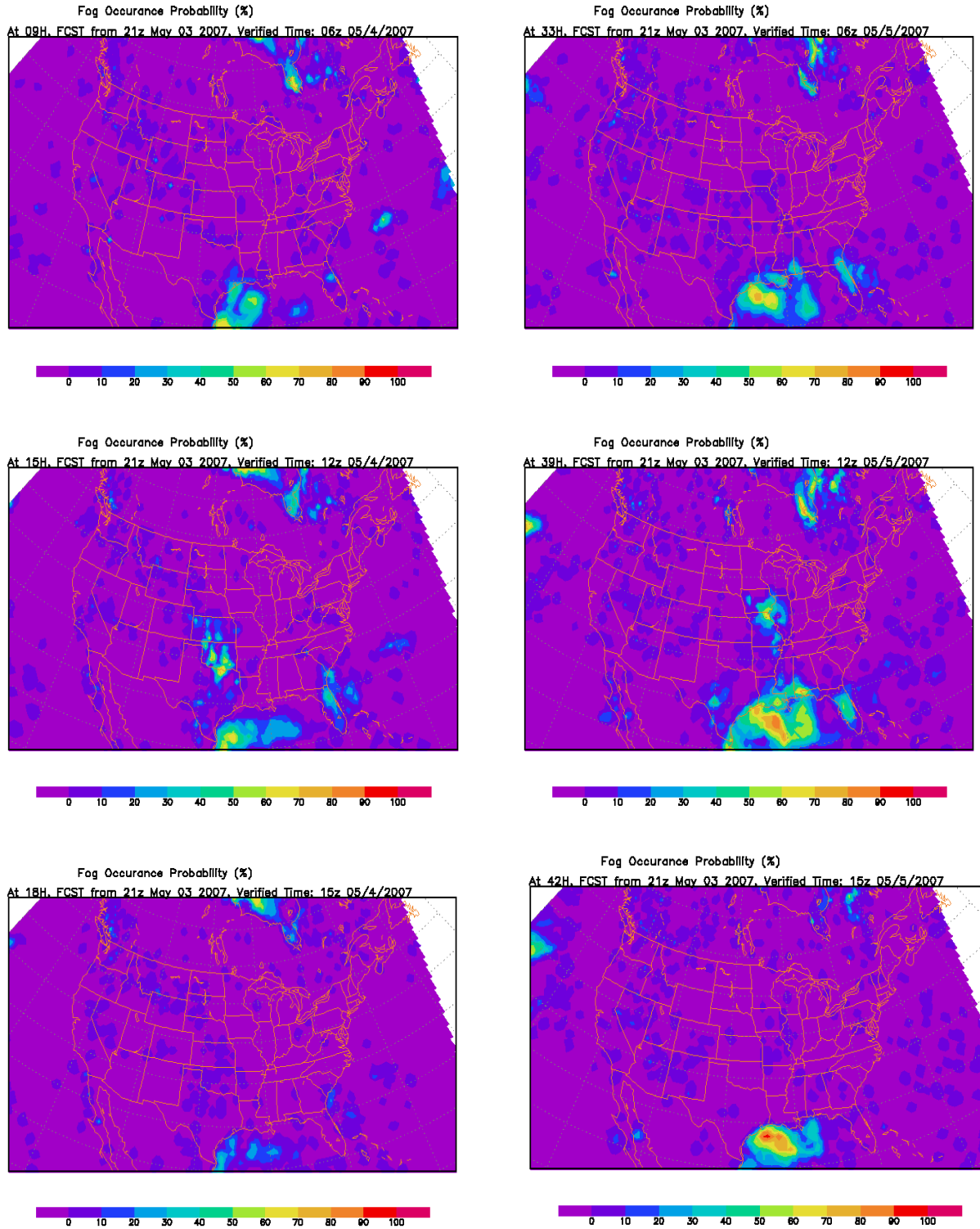
Figure 2. NCEP SREF fog occurrence probability forecast over CONUS, run for 21Z, May 3rd, 2007, and validated for the 9, 15, 18 hr forecasts (on May 4th, left column) and the 33, 39, 42 hr forecasts (on May 5th, right column), respectively.
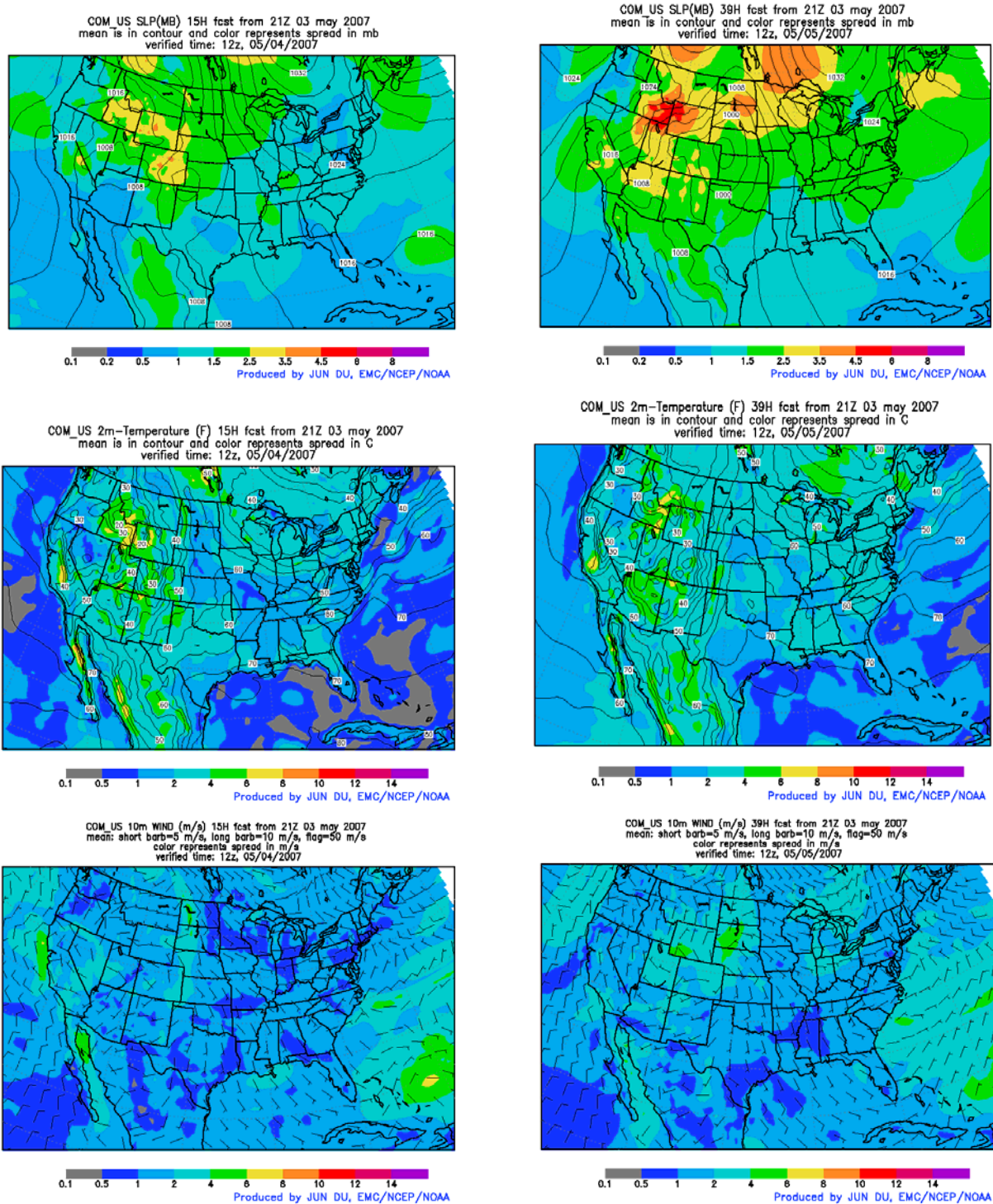
Figure 3. NCEP SREF ensemble mean of sea level pressure (top), 2m temperature (middle) and 10m wind speeds (bottom) over CONUS, run for 21Z, May 3rd, 2007, and validated for the 15 hr forecast (on May 4th, left column) and 39 hr forecast (on May 5th, right column), respectively.

As shown in Figure 3, the fog episodes also appeared in northern Florida and on the eastern coast of Georgia on May 4th, and in northern Florida on May 5th. These marine-radiation fogs were initially triggered by southeastern winds and moisture from the warmer ocean. The moist air met a cold tongue stretching down to Florida, as shown in Figure 3. The cooling was strengthened during the nights of May 3rd and 4th, leading to the formation of marine fogs on both days. But the fogs did not persist after daybreak. So both fogs were also of the radiation fog type.

2.3. Subjective verification

Because digital and grid observed fog data over such a large domain as the CONUS are still not available to us, objective verification of the fog forecasts could not be conducted now. But, subjective verification of the fogs over land or ocean could be performed with the satellite fog detection products produced by NOAA NESDIS. The satellite detection of fog recently emerged, based on the remote sensing of temperature from the 11mm and 4mm IR bands (Ellrod 2006). Current image files are generated for low stratus clouds or fog at night from GOES-11 or -12 or the NOAA AVHRR infrared channels. Two types of images were used to identify fogs over lands or oceans. The first is the low cloud base (LCB) image which helps to distinguish cloud bases below 1000 feet (about 300 m in red). Within the red area, fog is further identified by the cloud base height. The second type of image is fog depth, which can be used to directly to find the fog depth for some specific regions (such as some metro areas). These two types of images were combined to identify fogs. In this report, only the first type of images were used as truth for the subjective verification of the SREF ensemble fog forecast.

Figure. 4 shows the NESDIS low cloud base (LCB) detection images over the south central and the southeast CONUS on the mornings of May 4th and 5th, respectively. Comparing Figure 4 with middle panels in Figure 3, we can see that the ensemble forecast of fog over Texas-Oklahoma on May 4th was well confirmed by the satellite detections. The non-foggy forecast over the same region was also confirmed by the satellite detections on the second day. But the fog over the Texas coast was not well confirmed by the detection images, although there are large scale low clouds detected over the Gulf of Mexico on both May 4th and 5th. It should be noticed that the ensemble system predicts the fog occurrence *probability* rather than determining its occurrence. From the fog probability distributions over the Texas Gulf Coast, one may observe that the highest probability of fog occurrence is located offshore, particularly on May 5th. This means that the marine fog most likely appeared over the Gulf away from the coast.

Similarly, the fog occurrence probability forecasts over northern Florida and eastern Georgia were only about 30% on May 4th and 5th, and not 100%. The satellite detection images showed that there were only sparsely scattered fogs over northern Florida and the eastern coast of Georgia on May 4th and no fog at all on May 5th. From the probabilistic forecast point of view, the agreement between the lower fog occurrence probability and the sparsely scattered fogs detected over the same regions shows the reliability of the SREF fog forecast.
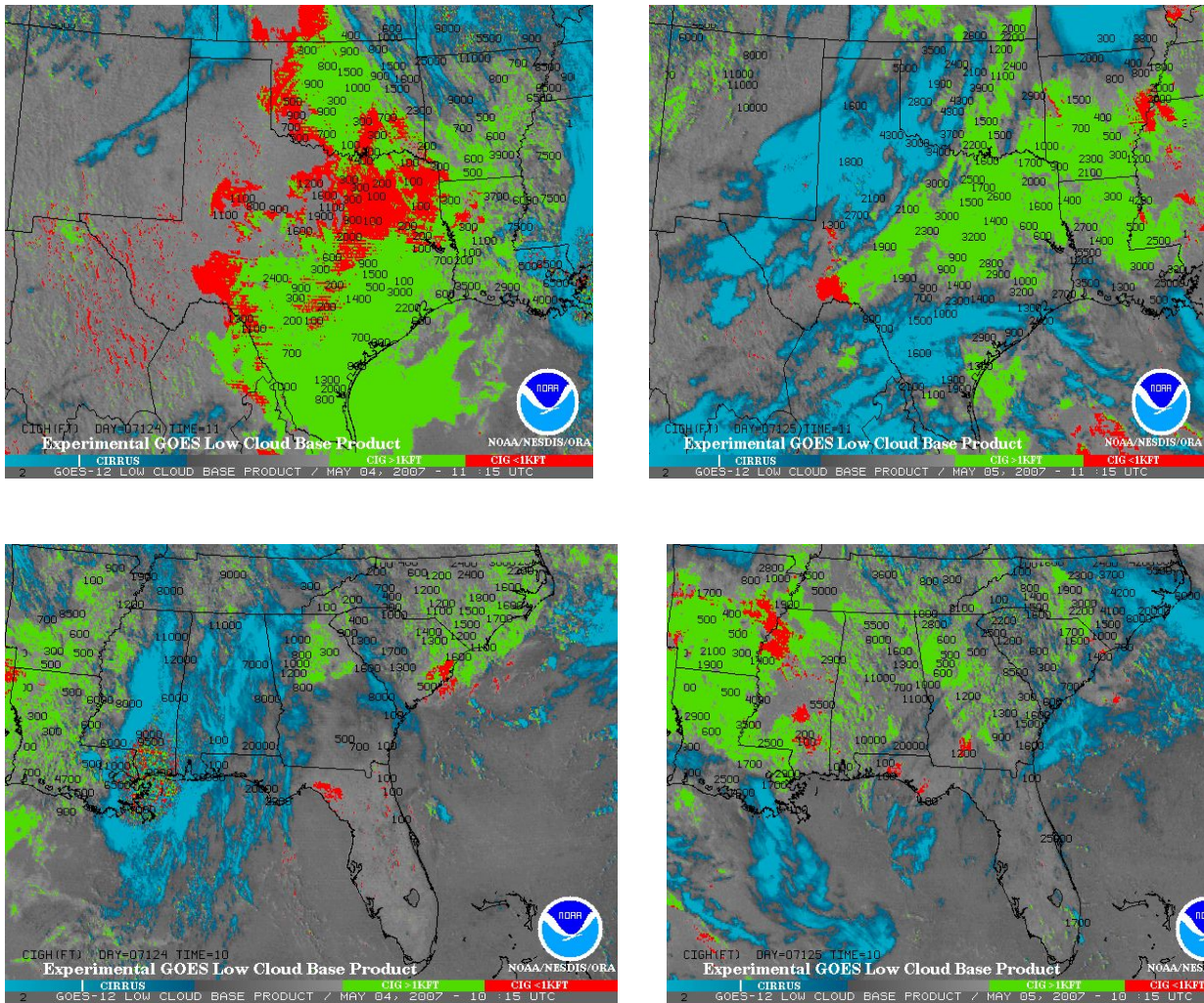
Figure 4. NOAA NESDIS GOES 12 low cloud base (LCB) detection images over south central (top) and the southeast (bottom) CONUS on the morning of May 4th (left) and 5th (right).

3. Asymptotic solution

As we know, conventional NWP models are not reliable nor skilful in predicting fog LWC near the surface. That is the reason why the SREF predicts the fog occurrence probability, rather than the fog intensity which requires modeled LWC at saturated grid points. Recently, we developed an asymptotic method for diagnosing fog conditions as well as the LWC (Zhou 2006). This method was based on the singular perturbation technique and an asymptotic analysis of steady radiation fog, from which a set of persistence conditions for

fog and LWC formulation were derived. After extending this work to include advection, it can potentially be applied in a conventional NWP forecast model. In this section, the extension is first briefly described and then applications in operational forecasts are suggested.

3.1. Asymptotic LWC formulation

Under the hypothesis of average cooling and turbulence within a saturated fog layer near the surface, the governing equation for the fog LWC can be written as the following partial differential equation (PDE)

$$\frac{\partial W(z,t)}{\partial t} = K\frac{\partial^2 W}{\partial z^2} - \frac{\partial G}{\partial z} + Adv + \beta(p,T)C_o, \quad (1)$$

where K is the layer-averaged turbulent exchange coefficient. G is the droplet gravitational settling flux onto the ground and can be expressed as $G = v_t W$, where v_t is the average droplet terminal velocity, parameterized as $-\alpha W$, and α is a tunable parameter that depends on the fog type. For radiation fog, $\alpha \sim 0.062$ (Brown et al. 1976). $Adv = -\vec{V} \cdot \nabla W$ is the horizontal advection of the LWC, where $\vec{V}$ is the horizontal wind vector. $\beta(p,T)C_o$ is the condensation rate per unit mass due to cooling of the air.

$C_o = -(\partial T / \partial t)$ is the layer-averaged local cooling rate, hereafter referred to as the cooling rate. The slope $\beta(p,T)$ can be expressed using the Clausius-Clapeyron equation

$$\beta(p,T) = \frac{622 L_v e_s(T)}{R_v T^2 p}, \quad (2).$$

where p and T are the air pressure and temperature. L_v and R_v, are the latent heat and the gas constant for vapor, respectively; e_s is the saturation vapor pressure.

Under steady fog conditions, the PDE (1) can be solved using the singular perturbation method. Following the procedure described by Zhou (2006), the asymptotic distribution of the fog LWC is

$$W(z,k) = \{\frac{[Adv + \beta(p,T)C_o]H}{\alpha}\}^{1/2}[(1-\frac{z}{H})^{1/2} - \frac{2}{1+e^{z/\delta}}] + O(K), \quad (3)$$

where

$$\delta = \frac{K}{2\{\alpha[Avd + \beta(p,T)C_o]H\}^{1/2}} \quad (4)$$

The $O(K)$ in (3) is the truncation error term, which can be omitted in application. The formulation (3) exhibits the water budget and the balance between local cooling, horizontal advection of liquid water, droplet gravitational settling and turbulence diffusion inside a steady fog layer. The $[Adv + \beta(p,T)C_o]$ is the producer of fog water, which must be positive. If an overall fog layer is in cooling status and the advection is positive (the upwind LWC is larger), LWC is steadily produced which is then transported to the ground by the droplet gravitational settling and the turbulence diffusion. But if the cooling rate or the advection decreases, or becomes negative (the upwind LWC is smaller), the overall LWC in the fog will decrease or be depleted completely.

The parameter δ can be considered as a *fog boundary layer* (FBL). The role of FBL is very similar to that of a mixing layer within a fog. When turbulence is very weak in its early stage, the FBL is very shallow, while as turbulence strengthens the FBL grows as predicted by Eq. (4). In this case, the LWC will decrease. It can be derived from (3) and (4) that when the turbulence intensity increases to such a critical level, or the FBL reaches the fog top (equivalent to destroying the inversion above the fog layer), the LWC will be completely exhausted. The *critical turbulence exchange coefficient* can be defined by the following persistence condition (Zhou 2006):

$$K < K_c = 1.38\{\alpha[Adv + \beta(p,T)C_o]\}^{1/2} H^{3/2}. \quad (5)$$

9

To keep the balance of liquid water in a steady fog, the turbulence intensity in the fog must be less than the critical turbulent exchange coefficient K_c, which is more sensitive to the fog depth ($H^{3/2}$) than to the cooling rate ($C_o^{1/2}$).

The inequality for the critical turbulent exchange coefficients in Eq. (5) defines the upper limit of turbulence intensity that a fog can withstand. An initial ground fog usually forms within 10 m of the surface and remains stable for a long time (pre-fog conditioning) if the surface turbulence does not exceed the critical turbulent exchange coefficients. Otherwise, the ground fog will dissipate. Several factors may cause the turbulence intensity to exceed K_c: (1) sunrise, which reduces the cooling rate and increases turbulence as well (K_c decreases and K increases); (2) local clouds moving over the fog region, which prevents the outgoing net radiation flux from the ground or the fog top and reduces the cooling rate inside the fog (K_c decreases); (3) warm advection, which also reduces the cooling rate (K_c decreases); (4) dry advection, which reduces the Adv (K_c decreases); and (5) rising local wind speeds, which increase the surface mechanical turbulence (K increases). On the contrary, an increase in cooling rate, a positive advection of the LWC, or cessation of turbulence will favor the persistence of ground fog.

As is indicated by (5) a deep fog (with a large H) has a large K_c, implying that it is not easy for turbulence to disperse a deep fog since a strong turbulence intensity is required to break the balance. For example, a uniform ground fog with $H \sim 2\ m$, $T = 10\ ^oC$ and a cooling rate $\sim 1\ ^oC\ hr^{-1}$, K_c is about $1.1\text{x}10^{-2}$ m^2s^{-1}. That is, if turbulence near the surface drops below $1.1\text{x}10^{-2}\ m^2s^{-1}$, a ground fog can persist. Otherwise, the ground fog will soon disappear, which is consistent with the typical turbulence intensity observed near the surface during the formation of radiation fog.

However, for a uniform deep fog with $H \sim 100$ m, K_c increases to 4 m^2s^{-1}. In other words, a 100m deep fog can persist in a very turbulent environment except when the turbulence intensity inside the fog bank exceeds 4 m^2s^{-1}. This explains why turbulence only disperses shallow fogs and not deep fogs observed by Fitzjarrald and Lala (1989).

The asymptotic solution (3) has a first-order approximation with respect to turbulence intensity K, so it is more accurate in conditions with weak turbulence than with strong turbulence. This can be confirmed by Figure 5, where the numerical solutions of PDE (1) and the asymptotic solutions under different values of K are compared. It is shown that the LWC profiles for the numerical and the asymptotic solutions are in close agreement with a small positive bias of 10% for weak turbulence and a larger positive bias of 30% for strong turbulence. But if the turbulence intensity further increases, being close to the critical threshold ($K_c \sim 0.51\ m^2s^{-1}$ in this case), both the asymptotic and the numerical LWC approach zero (Fig. 5c) at all levels.

Within a deep fog, the turbulence intensity usually grows from the ground as a result of warming in the lower parts of the fog. Thus, the uniform K hypothesis may not hold. The impact of the uniform K hypothesis on the asymptotic solution was evaluated by a comparison between two numerical solutions for a 100 m fog, one with K linearly increasing from zero at ground to a maximum value of 1.0 m^2s^{-1} at 70m and then linearly decreasing to zero at the top, and the other with a uniform K $\sim 0.5\ m^2s^{-1}$ representing an average of the first case. The result does not show a significant difference in the two LWC profiles (plot not presented here). So the uniform K assumption is not, at least in terms of solution accuracy, a serious problem when applying the solution in deep fogs.

As a fog grows deep, the maximum cooling rate lifts from the surface to the fog top and

warming emerges near the surface. To address such a distributed cooling pattern inside a deep fog, in the first order of approximation a linear vertical distribution of cooling rate can be assumed to solve the problem without much difficulty (Zhou 2006).
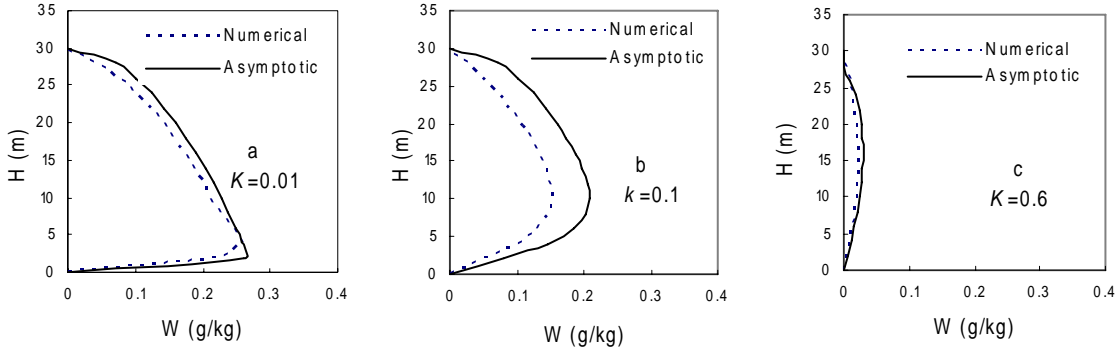
Figure 5. Comparisons between the steady solutions of PDE (1) with the asymptotic solutions for different turbulence exchange coefficients (in $m^2 s^{-1}$) for a uniform fog with $H \sim 30\ m$. In all cases, $T \sim 0.0\ ^oC$, cooling rate $\sim 1.0\ ^oC\ hr^{-1}$, for which, $Kc \sim 0.51\ m^2 s^{-1}$.

3.2. Applications of the asymptotic formulation

In Section 3.1, we have obtained two explicit formulations (3) and (5), which can be potentially applied to fog prediction. Since the cloud schemes are usually designed for clouds at high levels and not for fog near the ground, these formulations could be applied in a conventional NWP model to improve the fog prediction by diagnosing the fog persistence condition or resolving the fog LWC at saturated grid points near the surface. For example, if they are used inside a NWP model, the modeled cooling rate and turbulent exchange coefficient are used as input parameters. The depth of saturated layer is suggested for the fog depth. For a well-designed NWP model, the modeled cooling rate is comprehensive and has included all responsible contributions from radiation, turbulence, advection, grid-scale cloud water, etc,. If a grid point near the surface is saturated, the fog persistence condition at this best place is in its post processor. The fog condition or the LWC can be diagnosed or point is first checked with Eq. (5). If the condition is not satisfied, there is no fog. Even if it already has modeled fog at this point, its LWC is set to zero. If the saturated grid point meets the fog condition, its LWC is then resolved with formulation (3) instead of being simply converted from the excessive moisture. If the model already predicted fog, its LWC is treated as a first guess. Since the modeled cooling rate and turbulence reflect the impacts of the first guess fog, they are reliable enough to be used to resolve/adjust the first guess LWC at this point. Furthermore, the resolved LWC will be taken into account in the computations of cooling rate and turbulence in the next time steps of the model forecast. In such a two-way coupling, the interaction between the modeled cooling rate/turbulence and the resolved fog LWC can be adequately represented in the NWP model.

If it is used outside of a NWP model, the resolved based on the model output. But there will be no feedback of the resolved LWC into

the computation of these parameters in the following time steps. For a shallow saturated layer, this is not a severe problem since a shallow fog has less impact on its environment. But when the saturated layer grows deep, whether it has the modeled fog or not has a big impact on the modeled cooling rate and turbulence, and brings uncertainties into the resolved LWC.

The SREF fog prediction is generated from a set of operational mesoscale models and could be combined with asymptotic solutions (3) or (5) to (i) raise the forecast confidence by double-checking the fog condition at each foggy grid point and reducing the fault alarm rate, (ii) resolve the LWC if it indeed has fog at the saturated grid point, and (iii) reduce the missing rate by checking the fog condition at those "close-to" saturated points without modeled fog (bias correction for dry-bias members).

4. Summary

Operational fog forecasting over large domains, with either a sophisticated fog model coupled by a background mesoscale model or with a conventional NWP model, is very difficult and not realistic under current computing conditions. The first approach requires much more computing resources, while the second approach is not reliable in generating fog LWC near the surface. In this report we presented two solutions which could be applied centrally at NCEP. The first is an ensemble solution which has been implemented experimentally in the NCEP SREF system, but has no fog intensity forecast. The second solution is a diagnostic method which is based on a recently obtained asymptotic formulation.

The SREF fog ensemble forecast was briefly introduced and examined for an advection-radiation fog over Texas and Oklahoma, a marine fog over the Texas Gulf coast, and a marine-radiation fog over the Florida-Georgia coast on May 4th and 5th, 2007. Subjective verifications using the NOAA NESDIS satellite detections were conducted for these fog episodes, showing a general consistency between the forecasted fog events and the satellite detections in terms of ensemble probabilities and sparseness of detected fogs. However, the SREF fog product has no fog LWC output. To address this, the second solution could be applied. The applications inside and outside of a NWP model were tentatively described. Before actually implementing this method, it will need more experiments and testing.

In addition to the subjective verifications, objective verifications are also necessary to fully evaluate the SREF ensemble fog prediction. An objective verification of fog prediction over large domains requires gridded fog data such as observed visibility, dew point, and cloud base/top. The gridded fog data could come either from NOAA NESDIS or from Real Time Mesoscale Analysis (RTMA) and should be in GRIB-1 or GRIB-2 file format. We hope these data could be used in objective verifications of fog prediction in the near future.

References

Brown, R. and W. T. Roach, 1976: The physics of radiation fog: II – a numerical study. *Quart. J. Roy. Meteor. Soc*., **102**, 335-354.

Ellrod, G, 2006: Estimation of instrument cloud base conditions at night using GOES and surface temperature data. Available from http://www.orbit.nesdis.noaa.gov/smcd/opdb/aviation/opdb_pubs/avn00fog.htm

Du, J. and M. S. Tracton, 2001: Implementation of a real-time short-range ensemble forecasting system at NCEP: an update. Preprints, *9th Conference on Mesoscale Processes*, Ft. Lauderdale, Florida, Amer. Meteor. Soc., 355-356

Du, J., J. McQueen, G. DiMego, Z. Toth, D. Jovic, B. Zhou, and H. Chuang, 2006: New Dimension

of NCEP Short-Range Ensemble Forecasting (SREF) System: Inclusion of WRF Members, Preprint, *WMO Expert Team Meeting on Ensemble Prediction System*, Exeter, UK, Feb. 6-10, 2006. Available from http://www.wmo.int/web/www/DPFS/Meetings/ET-EPS_Exeter2006/DocPlan.html

Fitzjarrald, D. R. and G. G. Lala, 1989: Hudson valley fog environments. *J. Appl. Meteor.* **28**, 1303-1328.

Lewis, J. M., D. Koračin, , and K. T. Redmond, 2004: Sea Fog Research in the United Kingdom and United States: A Historical Essay Including Outlook. *Bull. Amer. Meteor. Soc*., **85**, 395-408.

Müller, M. D., M. Masbou, and A. Bott, Z. Janjic, 2005: Fog prediction in a 3D model with parameterized microphysics. Preprints, *World Weather Research Programme's Symposium on Nowcasting and Very Short Range Forecasting*, September 5-9, Toulouse, France.

Stoelinga, M. T. and T. T. Warner, 1999: Nonhydrostatic, mesobeta-scale model simulations of cloud ceiling and visibility for an east coast winter precipitation event. *J. Appl. Meteor*., **38**, 385-404.

Zhou, B. and Co-authors, 2004: An Introduction to NCEP SREF Aviation Project, CD-ROM, *11th Conference on Aviation, Range, and Aerospace*, Oct4-8, Hyannis, Amer. Meteor. Soc.

Zhou. B., 2006: Asymptotic solution of liquid water content equation at equilibrium state of radiation fog*, NCEP Office Note 450, National Centers for Environmental Prediction*. 41 pp. Available from http://www.emc.ncep.noaa.gov/officenotes/newernotes/on450.pdf